

Kepler-503b: An Object at the Hydrogen Burning Mass Limit Orbiting a Subgiant Star

CALEB I. CAÑAS,^{1, 2, 3} CHAD F. BENDER,⁴ SUVRATH MAHADEVAN,^{1, 2, 3} SCOTT W. FLEMING,⁵

THOMAS G. BEATTY,^{1, 2, 3} KEVIN R. COVEY,⁶ NATHAN DE LEE,^{7, 8} FRED R. HEARTY,¹

D. A. GARCÍA-HERNÁNDEZ,^{9, 10} STEVEN R. MAJEWSKI,¹¹ DONALD P. SCHNEIDER,^{1, 2} KEIVAN G. STASSUN,⁸
 AND ROBERT F. WILSON¹¹

¹Department of Astronomy & Astrophysics, The Pennsylvania State University, 525 Davey Lab, University Park, PA 16802, USA

²Center for Exoplanets & Habitable Worlds, University Park, PA 16802, USA

³Penn State Astrobiology Research Center, University Park, PA 16802, USA

⁴Department of Astronomy and Steward Observatory, University of Arizona, Tucson, AZ 85721, USA

⁵Space Telescope Science Institute, 3700 San Martin Dr., Baltimore, MD 21218, USA

⁶Department of Physics & Astronomy, Western Washington University, Bellingham, WA 98225, USA

⁷Department of Physics, Geology, and Engineering Technology, Northern Kentucky University, Highland Heights, KY 41099

⁸Department of Physics & Astronomy, Vanderbilt University, Nashville, TN 37235

⁹Instituto de Astrofísica de Canarias (IAC), E-38205 La Laguna, Tenerife, Spain

¹⁰Universidad de La Laguna (ULL), Departamento de Astrofísica, E-38206 La Laguna, Tenerife, Spain

¹¹Department of Astronomy, University of Virginia, Charlottesville, VA 22904, USA

ABSTRACT

Using spectroscopic radial velocities with the APOGEE instrument and *Gaia* distance estimates, we demonstrate that Kepler-503b, currently considered a validated *Kepler* planet, is in fact a brown-dwarf/low-mass star in a nearly circular 7.2-day orbit around a subgiant star. Using a mass estimate for the primary star derived from stellar models, we derive a companion mass and radius of $0.075 \pm 0.003 M_{\odot}$ ($78.6 \pm 3.1 M_{\text{Jup}}$) and $0.099_{-0.004}^{+0.006} R_{\odot}$ ($0.96_{-0.04}^{+0.06} R_{\text{Jup}}$), respectively. Assuming the system is coeval, the evolutionary state of the primary indicates the age is ~ 6.7 Gyr. Kepler-503b sits right at the hydrogen burning mass limit, straddling the boundary between brown dwarfs and very low-mass stars. More precise radial velocities and secondary eclipse spectroscopy with James Webb Space Telescope will provide improved measurements of the physical parameters and age of this important system to better constrain and understand the physics of these objects and their spectra. This system emphasizes the value of radial velocity observations to distinguish a genuine planet from astrophysical false positives, and is the first result from the SDSS-IV monitoring of Kepler planet candidates with the multi-object APOGEE instrument.

Keywords: binaries: eclipsing — stars: low-mass — techniques: spectroscopic; photometric

1. INTRODUCTION

Corresponding author: Caleb I. Cañas
 canas@psu.edu

The NASA *Kepler* space mission, in its search for transiting Earth analogues, provided nearly continuous observations of $\sim 200,000$ stars with a photometric precision of a few parts per million (Borucki et al. 2010; Koch et al. 2010). The

final *Kepler* data release (DR25) lists more than 8,000 objects of interest (KOIs), or targets showing a transit which may be caused by an exoplanet (Thompson et al. 2017). Vetting these KOIs has revealed over 2,000 eclipsing binaries with precise photometric data (Kirk et al. 2016). While high-resolution imaging (Furlan et al. 2017) and statistical methods (Morton et al. 2016) are useful for constraining the nature of a KOI, dynamical observations can provide an unambiguous classification for a given system.

Eclipsing binaries are important astrophysical systems because simultaneous modeling of spectroscopic and photometric observations yields precise dynamical masses and stellar radii (Torres et al. 2010). Precisely measured stellar parameters are valuable for calibrating and refining stellar evolution models (e.g., Fernandez et al. 2009; Torres et al. 2014) and even play a role in the cosmic distance scale. Furthermore, determining precise properties of exoplanets requires an understanding of their host stars’ parameters, particularly the masses and radii. The detection of false positive KOIs has greater implications for the planet-hosting stellar population. The presence of eclipsing binaries quantifies the false positive rate and can reveal any dependencies on parameters, such as the location within the *Kepler* field and properties of the host star or planetary candidate.

In this paper, we provide tight constraints on the age, radii, masses, and other properties of the low mass-ratio ($M_2/M_1 = q \sim 0.07$) eclipsing binary system Kepler-503 (KIC 3642741, 2MASS J19223275+3842276, $K_p = 14.75$, $H = 13.14$). The paper is structured as follows: Section 2 presents the observational data, Section 3 discusses our data processing, and Section 4 describes our analysis. A discussion of our results is presented in Section 5.

2. OBSERVATIONS

Kepler-503 was observed from Apache Point Observatory (APO) between 30 April 2015 and 7 April 2017 as part of the APO Galaxy Evolution Experiment (APOGEE) KOI program (Fleming et al. 2015; Majewski et al. 2017; Zasowski et al. 2017) within SDSS-IV (Blanton et al. 2017). We obtained nineteen spectra of Kepler-503, using the high-resolution ($R \sim 22500$), near-infrared ($1.514 - 1.696 \mu\text{m}$), multi-object APOGEE spectrograph (Wilson et al. 2010, 2012), mounted on the Sloan 2.5-meter telescope (Gunn et al. 2006). The observations are summarized in Table 1, which lists our derived radial velocities, their uncertainties (corresponding to a $1 - \sigma$ error), and the signal-to-noise ratio (SNR) per pixel for each epoch. One observation with a SNR below 10 was not used for analysis.

Table 1. APOGEE Observations

$\text{BJD}_{\text{TDB}}^{\dagger}$	RV (km s $^{-1}$)	$1 - \sigma$ (km s $^{-1}$)	SNR ‡ (pixel $^{-1}$)
2456932.708196	-52.86	0.21	22
2457142.860499	-52.11	0.2	24
2457199.743627	-46.26	0.35	12
2457264.658553	-43.3	0.24	17
2457265.795423	-50.02	0.17	29
2457266.783228	-52.86	0.18	25
2457294.705133	-49.98	0.17	30

Table 1 continued

Table 1 (continued)

BJD _{TDB} [†]	RV (km s ⁻¹)	1- σ (km s ⁻¹)	SNR [‡] (pixel ⁻¹)
2457319.648315	-45.49	0.25	19
2457472.004760	-45.25	0.26	16
2457498.977450	-52.66	0.39	12
2457527.949126	-53.05	0.15	33
2457554.814754	-42.62	0.26	16
2457562.871095	-47.25	0.26	16
2457643.740360	-52.13	0.35	12
2457672.675784	-52.15	0.17	27
2457701.553540	-51.51	0.49	12
2457831.992227	-50.48	0.23	17
2457850.990495	*	*	6

[†]BJD_{TDB} is the Barycentric Julian Date in the Barycentric Dynamical Time standard, which takes into consideration relativistic effects.

[‡]APOGEE has about two pixels per resolution element.

*Value omitted for the observation with SNR < 10.

Kepler-503 was observed for the entirety of the *Kepler* mission, is listed as a planetary candidate in DR25, and was statistically validated as an exoplanet by Morton et al. (2016). The final data release lists a shallow, 0.37% transit signal with an orbital period of 7.258450123 days and an estimated physical radius of $5.53_{-0.53}^{+1.59}$ R_⊕. The stellar parameters in the DR25 stellar properties catalog (Mathur et al. 2017) were derived with photometric priors and inferred from stellar models. The DR25 parameters for Kepler-503 suggest a solar-like host star with an effective temperature of 5638_{-171}^{+154} K, a mass of $1.006_{-0.120}^{+0.090}$ M_⊕, and a radius of $0.920_{-0.088}^{+0.264}$ R_⊕.

3. DATA PROCESSING

3.1. Radial Velocities

The APOGEE data reduction pipeline (Nidever et al. 2015) performs sky subtraction, telluric and barycentric correction, and wavelength and flux calibration for each observation of a target. We focused our analysis on these individual spectra for

dynamical characterization. While the APOGEE pipeline provides radial velocity measurements, we performed additional post-processing on the spectrum to remove residual telluric lines prior to analysis.

Radial velocities of Kepler-503 were derived using the cross-correlation method with uncertainties calculated via the maximum-likelihood approach presented by Zucker (2003). With this method, we account for uncertainty contributions from the spectral bandwidth, sharpness of the correlation peak, and the spectral line SNR but cannot exclude systematic uncertainties due to the instrument or poor template selection. Cross-correlation searches for the Doppler shift of an observed spectrum that maximizes the correlation with a template that adequately represents the observed spectrum without a Doppler shift. The best-fitting spectrum should have the highest correlation and it is common practice for this to be used as the template (e.g., Latham et al. 2002). We identified the best-fitting synthetic spectrum in the H-band from a grid of BT-Settl synthetic spectra (Allard et al. 2012)

by cross-correlating the APOGEE epoch with the highest SNR against a grid spanning surface effective temperature ($5100 \leq T_e \leq 6100$, in intervals of 100 K), surface gravity ($3.5 \leq \log g \leq 4.5$, in intervals of 0.5 dex), metallicity ($-0.5 \leq [\text{M}/\text{H}] \leq 0.5$, in intervals of 0.5 dex), and rotational broadening ($2 \leq v \sin i \leq 50$, in intervals of 2 km s^{-1}). The synthetic spectrum with the largest correlation was used for the final cross-correlation to derive the reported radial velocities in Table 1. The properties of the best model are listed in Table 2 and were not used as priors for fitting the system.

3.2. Photometry

We used the *Kepler* pre-search data conditioned time-series light curves (Smith et al. 2012; Stumpe et al. 2012, 2014) available at the Mikulski Archive for Space Telescopes (MAST). We assumed the transit signal was superimposed on the stellar variability and could be modeled using a Gaussian process. We used the `celerite` package and assumed a quasi-periodic covariance function for the Gaussian process, following the procedure in Foreman-Mackey et al. (2017). No additional processing was performed on the light curve.

4. RESULTS

We jointly modeled Kepler-503’s radial velocities and light curve using the EXOFASTv2 analysis package (Eastman 2017). The light curve and Keplerian radial velocity models follow the parametrization described by Eastman et al. (2013). We adopted a quadratic limb darkening law for the transit. The priors for the modeling

included (i) 2MASS *JHK* magnitudes (Skrutskie et al. 2006), (ii) SDSS *ugriz* magnitudes (Alam et al. 2015), (iii) *UBV* magnitudes (Everett et al. 2012), (iv) WISE magnitudes (Wright et al. 2010), (v) surface gravity, temperature and metallicity from the APOGEE Stellar Parameter and Chemical Abundances Pipeline (ASPCAP, García Pérez et al. 2016), (vi) the maximum visual extinction from estimates of Galactic dust extinction by Schlafly & Finkbeiner (2011), (vii) the photometric measurements from the second data release of the *Gaia* survey (Gaia Collaboration et al. 2018), and (viii) the distance estimate from Bailer-Jones et al. (2018). We validated the performance of our EXOFASTv2 implementation by analyzing the corresponding data products for KOI-189, and obtained very similar parameters to those published by Díaz et al. (2014) using the `PASTIS` planet-validation software. We repeated the analysis for Kepler-503 using the parallax from *Gaia* to determine if there were any significant effects from the nonlinearity of the parallax transformation or any asymmetry in the parallax posterior distribution. The results are consistent to within their $1 - \sigma$ uncertainties and herein we present values from the analysis using the distance prior. Figure 1 presents the result of the fit and Table 2 provides a summary of the stellar priors and the inferred systemic parameters along with their confidence intervals. The minimum companion mass is $\sim 0.075 M_{\odot}$, a value incompatible with the statistical validation and estimated parameters from DR25.

Table 2. Parameters for the Kepler-503 System

Parameter	Units	Median Value
Primary Synthetic Spectrum [†] :		
Effective Temperature	T_e (K)	6000

Table 2 continued

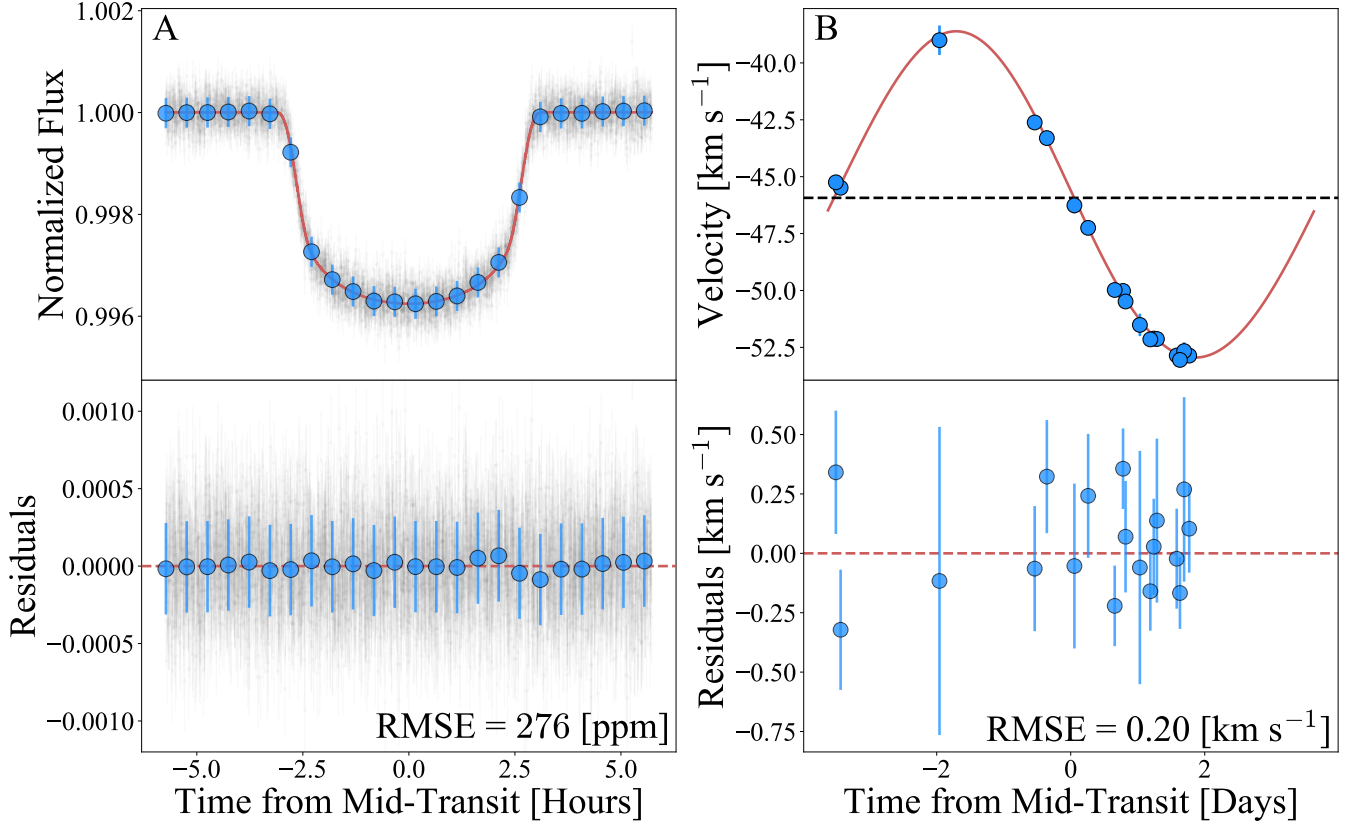


Figure 1. The photometry and velocimetry of Kepler-503. Panel A displays the phase-folded photometry from DR25. The small dots are the raw data while the larger circles are binned to the *Kepler* long-cadence. Panel B shows the radial velocities from Table 1 phased to the period of the system. In each case, the top panel contains the model as a solid line while the bottom panel shows the residuals and the root mean square error. The derived mass and radius ratios are $M_2/M_1 = 0.0648$ and $R_2/R_1 = 0.05619$, respectively. The modeled stellar parameters for the host star, Kepler-503A, give properties of the secondary companion that are incompatible with that of an exoplanet.

Table 2 (continued)

Parameter	Units	Median Value
Surface Gravity	$\log(g_1)$ (cgs) ..	4.0
Metallicity	[M/H]	0.0
Rotational Velocity	$v \sin i$ (km s ⁻¹)	2.0
Primary Stellar Priors:		
Effective Temperature [‡]	T_e (K)	5690 ± 150
Surface Gravity [‡]	$\log(g_1)$ (cgs) ..	4.0
Metallicity [‡]	[Fe/H]	0.17 ± 0.05
Maximum Visual Extinction	$A_{V,max}$	0.43
Distance	(pc)	1628 ± 55

Table 2 continued

Table 2 (*continued*)

Parameter	Units	Median Value
Primary Parameters:		
Mass	M_1 (M_\odot)	$1.154^{+0.047}_{-0.042}$
Radius	R_1 (R_\odot)	$1.764^{+0.080}_{-0.068}$
Density	ρ_1 (g cm^{-3}) ..	$0.297^{+0.038}_{-0.037}$
Surface Gravity	$\log(g_1)$ (cgs) .	4.008 ± 0.038
Effective Temperature	T_e (K)	5670^{+100}_{-110}
Metallicity	[Fe/H]	$0.169^{+0.046}_{-0.045}$
Age	(Gyr)	$6.7^{+1.0}_{-0.9}$
Parallax	(mas)	$0.617^{+0.020}_{-0.019}$
Secondary Parameters:		
Mass	M_2 (M_\odot)	0.075 ± 0.003
Radius	R_2 (R_\odot)	$0.099^{+0.006}_{-0.004}$
Density	ρ_2 (g cm^{-3}) ..	108 ± 17
Surface Gravity	$\log(g_2)$ (cgs) .	$5.320^{+0.045}_{-0.050}$
Equilibrium Temperature	T_{eq} (K)	1296^{+22}_{-23}
Orbital Parameters:		
Orbital Period	P (days)	7.2584481 ± 0.0000023
Time of Periastron	T_P (BJD _{TDB}) .	$2454970.27^{+0.63}_{-1.1}$
Semi-major Axis	a (AU)	0.0786 ± 0.0010
Orbital Eccentricity	e	$0.025^{+0.014}_{-0.012}$
Argument of Periastron	ω (degrees) ..	33^{+32}_{-54}
Semi-amplitude Velocity	K (km s^{-1}) ..	7.17 ± 0.18
Mass Ratio	q	$0.0648^{+0.0019}_{-0.0020}$
Systemic Velocity	γ (km s^{-1}) ..	-45.93 ± 0.10
Radial Velocity Jitter	σ_{RV} (m s^{-1}) ..	168^{+96}_{-92}
Transit Parameters:		
Time of Mid-transit	T_C (BJD _{TDB}) .	$2454971.34494 \pm 0.00026$
Radius Ratio	R_2/R_1	$0.05619^{+0.00069}_{-0.00060}$
Scaled Semi-major Axis	a/R_1	$9.59^{+0.39}_{-0.42}$
$\text{ecos}\omega$	$0.017^{+0.009}_{-0.010}$
$\text{esin}\omega$	$0.010^{+0.020}_{-0.015}$
Linear Limb-darkening Coefficient ...	u_1	0.419 ± 0.023

Table 2 continued

Table 2 (*continued*)

Parameter	Units	Median Value
Quadratic Limb-darkening Coefficient	u_2	$0.238^{+0.044}_{-0.045}$
Orbital Inclination	i (degrees) . . .	$88.04^{+1.0}_{-0.76}$
Impact Parameter	b	$0.32^{+0.11}_{-0.17}$

[†]These parameters are for the best-fit template spectrum used for cross-correlation.

[‡]These values are from ASPCAP.

The stellar parameters from EXOFASTv2 are derived using stellar models; the values suggest Kepler-503 is an evolved star beyond the terminal age main sequence. Seager & Mallén-Ornelas (2003) proposed a diagnostic for a transiting system using transit parameters to obtain an estimate of the primary stellar density (ρ_1). With both photometry and velocimetry, one can determine that the observational data are consistent with the selected stellar models (e.g., von Boetticher et al. 2017). To determine if the deviation from the DR25 stellar parameters was justified, we used the MESA Isochrones & Stellar Tracks (MIST, Dotter 2016; Choi et al. 2016) to model the primary star and iteratively refine its parameters until the density derived from the photometry and velocimetry was within the uncertainty of the density from the models.

The result of the stellar modeling is shown in Figure 2 and demonstrates that the stellar parameters are comparable to those derived with EXOFASTv2. The data demonstrate that the primary star, Kepler-503, is not a solar analogue, but instead a slightly evolved subgiant. When compared to stellar evolution models, the posterior distributions for the primary star surface effective temperature and luminosity are located in the subgiant branch, which is in agreement with a slightly evolved system. Accordingly, these stellar parameters suggest that the purported exoplanet is actually an object near the hydrogen burning limit of $\sim 0.075 M_{\odot}$ (e.g., Chabrier et al. 2005).

5. DISCUSSION

5.1. Constraint on the Companion Age

Kepler-503, and particularly the secondary component, is of great astrophysical interest because the age of a star is a fundamental parameter that is often poorly constrained. This situation forces age estimates to rely on proxies, such as magnetic activity, element depletion, rotation (gyrochronology, e.g., Soderblom 2010), or asteroseismology (e.g., Pinsonneault et al. 2018), which are difficult to measure for objects like Kepler-503b. This measurement is further complicated in low-mass stars because their spindown timescales can exceed the age of the Galaxy (West et al. 2008), and their fully convective nature can deplete lithium after only a few hundred million years (Stauffer et al. 1998). Objects near the bottom of the stellar mass function are of interest because they define the transition from bona fide stars to planets. The simplest way to determine the age of such an object is to associate it with another star or group for which the age is better constrained. Here, we assume Kepler-503 is a coeval system. The subgiant nature of the primary star places a strong constraint on the age of the companion because the placement of the subgiant branch on the Hertzsprung-Russell diagram is allowed for only a limited age range, according to stellar evolution models (e.g., Soderblom 2010). The modeling suggests the age of the Kepler-503 system is $6.7^{+0.9}_{-1.0}$ Gyr, making it considerably older than the Solar System.

5.2. Constraints on the Companion Temperature

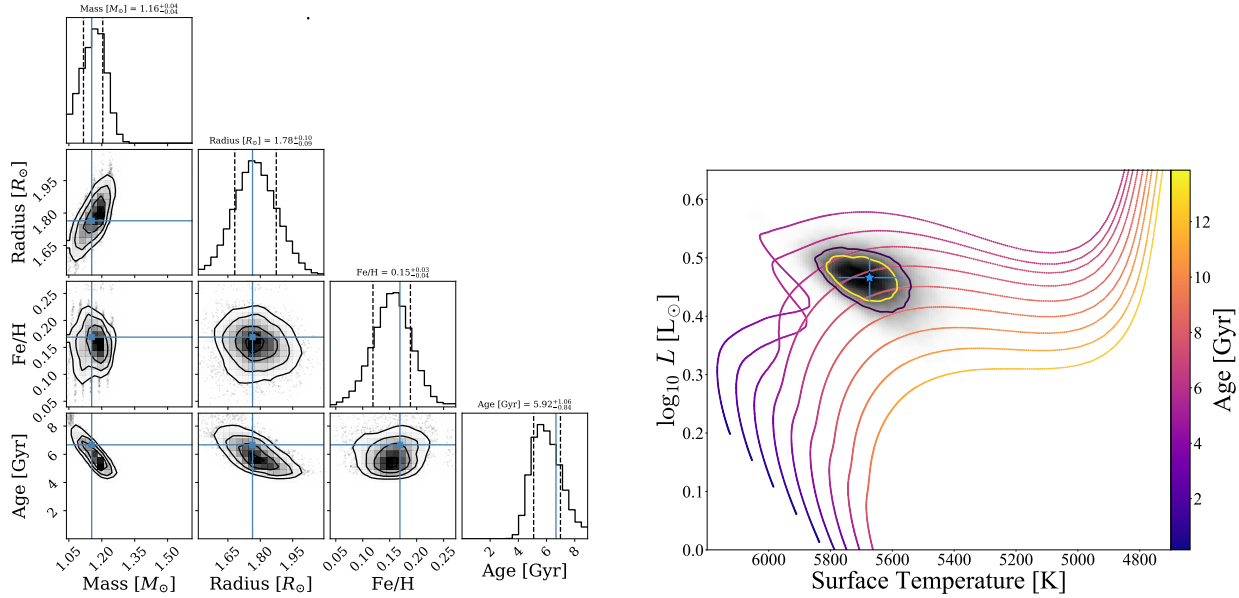


Figure 2. The stellar parameters for the host star Kepler-503A. The left panel shows the posterior distribution for physical parameters of Kepler-503A after modeling various photometric parameters with MIST models. The values derived from EXOFASTv2 using the Yale-Yonsei isochrones are marked with lines for clarity. The models suggest Kepler-503A is an evolved subgiant star. The right panel shows the placement of the primary star on a Hertzsprung-Russel Diagram. The two-dimensional kernel density estimate of the posterior distribution from the EXOFASTv2 fit is included for reference. MIST evolution tracks are indicated for masses between 1.0 and 1.2 M_{\odot} in steps of 0.025 M_{\odot} and are shaded according to age. The placement of Kepler-503A is consistent with a star near the subgiant branch.

The lack of a secondary eclipse in the photometry provides additional information about Kepler-503b. The dearth of an eclipse, despite the low eccentricity and inclination of the orbit, places a constraint on the companion’s effective surface temperature. The estimated eclipse depth is a function of both the radius ratio, R_2/R_1 , and the surface brightness ratio, B_2/B_1 . Using the parameters derived in this paper, the equilibrium temperature of Kepler-503b is ~ 1296 K. For such an object, the estimated transit depths for *Spitzer*’s 3.6 and 4.5 μm band-passes are ~ 150 and ~ 220 ppm, respectively. Even if we were to assume a higher surface effective temperature that is appropriate for a very low-mass star (~ 2300 K), the estimated eclipse depths for Kepler-503 are at the sensitivity limits of these *Spitzer* channels. For *Kepler*, the estimated eclipse depth at 600 nm is < 1 ppm and is dwarfed by the variance in the light curve. Future photometric and spectroscopic observations with the James Webb Space Telescope are required

to further constrain the flux ratio of the system to better characterize Kepler-503b.

5.3. Constraints on Evolutionary Models

The study of objects similar to Kepler-503b is critical for the empirical calibration of the mass-radius relation near the hydrogen burning mass limit ($\sim 0.075 M_{\odot}$). Figure 3 shows posterior distribution of Kepler-503b on a mass-radius diagram for brown dwarfs and low-mass stars. Its mass and radius are comparable to those of the brown dwarf KOI-189b (Díaz et al. 2014), with values that span the boundary between L- and M-dwarfs. Kepler-503b is one of the few objects in the regime where evolutionary tracks converge, and can thus help refine said models. The properties of Kepler-503b appear consistent with evolutionary tracks for solar metallicity low-mass stars and brown dwarfs. From the L- and T-dwarf models by Saumon & Marley (2008), the 5 and 10 Gyr evolutionary tracks are the best matches for this

object. One caveat is that, while the derived metallicity for the host star suggests this is a slightly metal-rich system, the cloud-based models exist only for solar metallicities. Given the recent interest in very low-mass stars as targets for exoplanet searches (e.g., Gillon et al. 2017), it is essential that the super-solar metallicity regime be properly characterized. Future searches for planets around ultra-cool dwarfs will require precise masses and radii of the host star to properly characterize any detected exoplanets.

6. SUMMARY

This paper reveals a low mass-ratio eclipsing binary system in a nearly circular orbit that was erroneously classified as a transiting exoplanet. Analysis of the photometric and spectroscopic data shows Kepler-503 is an old system with a companion at the hydrogen burning mass limit. This misclassification is largely due to the stellar parameters previously adopted (i.e., a solar-like host). The stellar classification from DR25 used a prior which is known to underestimate the number of sub-giants due to Malmquist bias (e.g., Bastien et al. 2014). Mathur et al. (2017) acknowledge that some systematic biases persist in the DR25 stellar properties catalog, resulting in misclassified systems such as Kepler-503.

This study is one example of the systems observed in the ongoing APOGEE KOI program, with the ultimate goal of (i) refining the false positive rate of *Kepler* exoplanet candidates, (ii) revealing any dependencies with stellar or candidate parameters, and (iii) understanding binarity and its effect in the planet host population. The recent second data release from the *Gaia* survey will be helpful for future validation of KOIs by providing a parallax that help to constrain the properties of the host star.

CIC, CFB, and SM acknowledge support from NSF award AST 1517592. ND, SRM, and RFW would like to acknowledge support from NSF Grant Nos. 1616684 and 1616636. DAGH ac-

knowledges support provided by the Spanish Ministry of Economy and Competitiveness (MINECO) under grant AYA-2017-88254-P. Some of the data presented in this paper were obtained from MAST. STScI is operated by the Association of Universities for Research in Astronomy, Inc., under NASA contract NAS5-26555. Support for MAST for non-HST data is provided by the NASA Office of Space Science via grant NNX09AF08G and by other grants and contracts. 2MASS is a joint project of the University of Massachusetts and IPAC at Caltech, funded by NASA and the NSF. Funding for the *Kepler* mission is provided by the NASA Science Mission directorate. The NASA Exoplanet Archive is operated by Caltech, under contract with NASA under the Exoplanet Exploration Program.

Funding for SDSS-IV has been provided by the Alfred P. Sloan Foundation, the U.S. Department of Energy Office of Science, and the Participating Institutions. SDSS-IV acknowledges support and resources from the Center for High-Performance Computing at the University of Utah. The SDSS web site is www.sdss.org. SDSS-IV is managed by the Astrophysical Research Consortium for the Participating Institutions of the SDSS Collaboration including the Brazilian Participation Group, the Carnegie Institution for Science, Carnegie Mellon University, the Chilean Participation Group, the French Participation Group, Harvard-Smithsonian Center for Astrophysics, Instituto de Astrofísica de Canarias, The Johns Hopkins University, Kavli Institute for the Physics and Mathematics of the Universe (IPMU) / University of Tokyo, Lawrence Berkeley National Laboratory, Leibniz Institut für Astrophysik Potsdam (AIP), Max-Planck-Institut für Astronomie (MPIA Heidelberg), Max-Planck-Institut für Astrophysik (MPA Garching), Max-Planck-Institut für Extraterrestrische Physik (MPE), National Astronomical Observatories of China, New Mexico State University, New York University, University of Notre Dame, Observatório Nacional / MCTI,

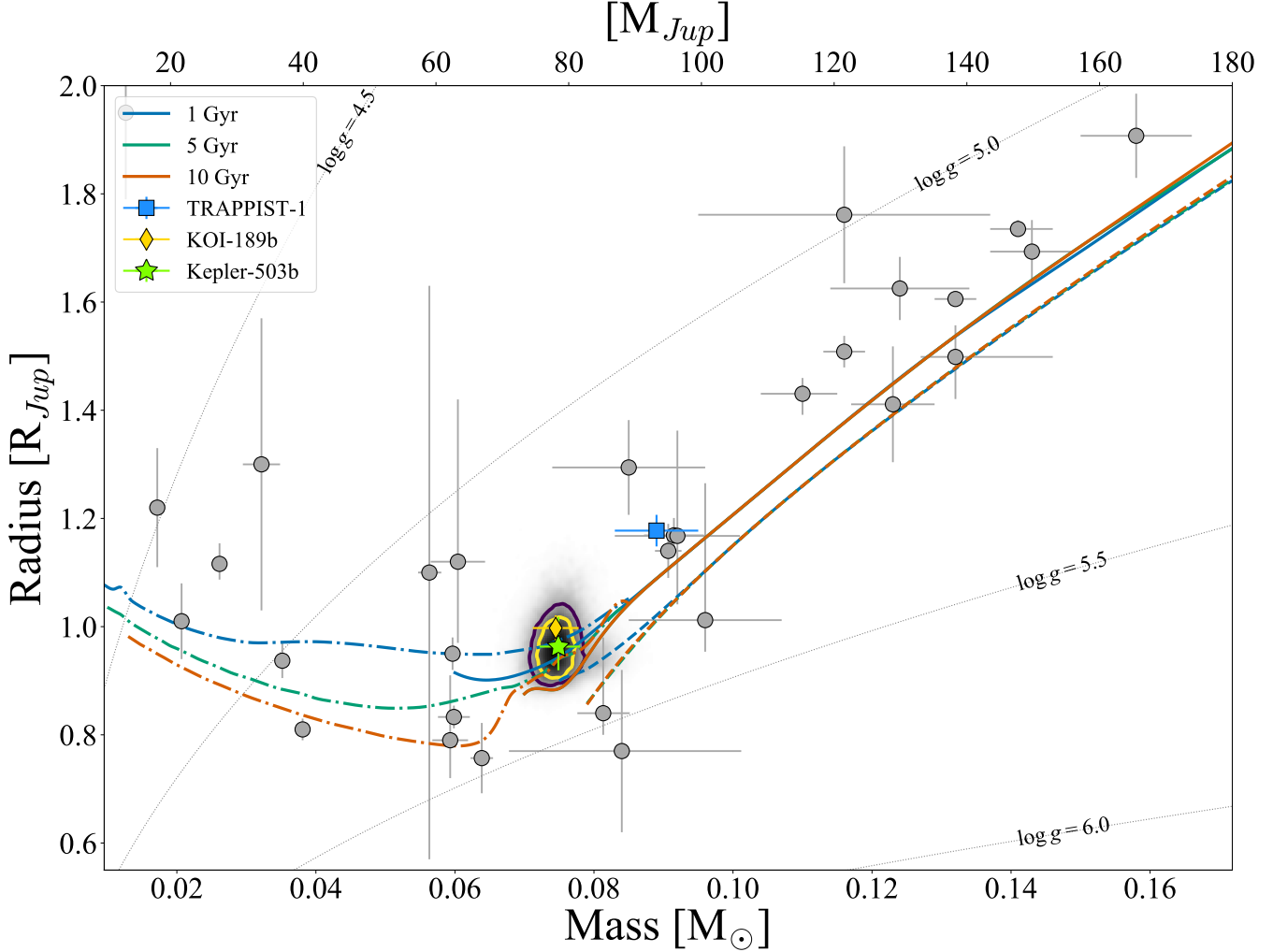


Figure 3. The mass and radius posterior distribution of the companion, Kepler-503b. Kepler-503b is not an Earth-size planet but an object near the hydrogen burning mass limit. The parameters derived for Kepler-503b are plotted along a two-dimensional kernel density estimate of the posterior distribution from our fit. The contours represent the $1-\sigma$ and $2-\sigma$ ($\sim 39.3\%$ and $\sim 63.2\%$ of the volume, respectively). For reference, the very low-mass star TRAPPIST-1 and the brown dwarf KOI-189b are plotted as a square and diamond, respectively, while other low-mass stars and high-mass sub-stellar companions from the literature appear as circles (see [von Boetticher et al. 2017](#)). Lines of constant surface gravity are drawn and masses are given in both solar and Jovian units. Models for sub-stellar companions and low-mass stars span the ages 1, 5, and 10 Gyr. The solid lines are evolutionary tracks from [Baraffe et al. \(2015\)](#) assuming solar metallicity ($[M/H] = 0.0$), the dashed lines are from [Baraffe et al. \(1998\)](#) assuming sub-solar metallicity ($[M/H] = -0.5$), and the dash-dotted lines are from [Saumon & Marley \(2008\)](#) for L- and T-dwarfs assuming solar metallicity and a hybrid cloudy/cloudless evolutionary sequence. This figure is adapted from [von Boetticher et al. \(2017\)](#).

The Ohio State University, Pennsylvania State University, Shanghai Astronomical Observatory, United Kingdom Participation Group, Universidad Nacional Autónoma de México, University of Arizona, University of Colorado Boulder, Univer-

sity of Oxford, University of Portsmouth, University of Utah, University of Virginia, University of Washington, University of Wisconsin, Vanderbilt University, and Yale University.

REFERENCES

Alam, S., Albareti, F. D., Allende Prieto, C., et al. 2015, *ApJS*, **219**, 12

Allard, F., Homeier, D., & Freytag, B. 2012, *Philosophical Transactions of the Royal Society of London Series A*, **370**, 2765

Bailer-Jones, C. A. L., Rybizki, J., Fouesneau, M., Mantelet, G., & Andrae, R. 2018, ArXiv e-prints, [arXiv:1804.10121 \[astro-ph.SR\]](https://arxiv.org/abs/1804.10121)

Baraffe, I., Chabrier, G., Allard, F., & Hauschildt, P. H. 1998, *A&A*, **337**, 403

Baraffe, I., Homeier, D., Allard, F., & Chabrier, G. 2015, *A&A*, **577**, A42

Bastien, F. A., Stassun, K. G., & Pepper, J. 2014, *ApJL*, **788**, L9

Blanton, M. R., Bershadsky, M. A., Abolfathi, B., et al. 2017, *AJ*, **154**, 28

Borucki, W. J., Koch, D., Basri, G., et al. 2010, *Science*, **327**, 977

Chabrier, G., Baraffe, I., Allard, F., & Hauschildt, P. H. 2005, ArXiv Astrophysics e-prints, [astro-ph/0509798](https://arxiv.org/abs/astro-ph/0509798)

Choi, J., Dotter, A., Conroy, C., et al. 2016, *ApJ*, **823**, 102

Díaz, R. F., Montagnier, G., Leconte, J., et al. 2014, *A&A*, **572**, A109

Dotter, A. 2016, *ApJS*, **222**, 8

Eastman, J. 2017, EXOFASTv2: Generalized publication-quality exoplanet modeling code, Astrophysics Source Code Library, [ascl:1710.003](https://ascl.net/1710.003)

Eastman, J., Gaudi, B. S., & Agol, E. 2013, *PASP*, **125**, 83

Everett, M. E., Howell, S. B., & Kinemuchi, K. 2012, *PASP*, **124**, 316

Fernandez, J. M., Latham, D. W., Torres, G., et al. 2009, *ApJ*, **701**, 764

Fleming, S. W., Mahadevan, S., Deshpande, R., et al. 2015, *AJ*, **149**, 143

Foreman-Mackey, D., Agol, E., Ambikasaran, S., & Angus, R. 2017, *AJ*, **154**, 220

Furlan, E., Ciardi, D. R., Everett, M. E., et al. 2017, *AJ*, **153**, 71

Gaia Collaboration, Brown, A. G. A., Vallenari, A., et al. 2018, ArXiv e-prints, [arXiv:1804.09365](https://arxiv.org/abs/1804.09365)

García Pérez, A. E., Allende Prieto, C., Holtzman, J. A., et al. 2016, *AJ*, **151**, 144

Gillon, M., Triaud, A. H. M. J., Demory, B.-O., et al. 2017, *Nature*, **542**, 456

Gunn, J. E., Siegmund, W. A., Mannery, E. J., et al. 2006, *AJ*, **131**, 2332

Kirk, B., Conroy, K., Prša, A., et al. 2016, *AJ*, **151**, 68

Koch, D. G., Borucki, W. J., Basri, G., et al. 2010, *ApJL*, **713**, L79

Latham, D. W., Stefanik, R. P., Torres, G., et al. 2002, *AJ*, **124**, 1144

Majewski, S. R., Schiavon, R. P., Frinchaboy, P. M., et al. 2017, *AJ*, **154**, 94

Mathur, S., Huber, D., Batalha, N. M., et al. 2017, *ApJS*, **229**, 30

Morton, T. D., Bryson, S. T., Coughlin, J. L., et al. 2016, *ApJ*, **822**, 86

Nidever, D. L., Holtzman, J. A., Allende Prieto, C., et al. 2015, *AJ*, **150**, 173

Pinsonneault, M. H., Elsworth, Y. P., Tayar, J., et al. 2018, ArXiv e-prints, [arXiv:1804.09983 \[astro-ph.SR\]](https://arxiv.org/abs/1804.09983)

Saumon, D., & Marley, M. S. 2008, *ApJ*, **689**, 1327

Schlafly, E. F., & Finkbeiner, D. P. 2011, *ApJ*, **737**, 103

Seager, S., & Mallén-Ornelas, G. 2003, *ApJ*, **585**, 1038

Skrutskie, M. F., Cutri, R. M., Stiening, R., et al. 2006, *AJ*, **131**, 1163

Smith, J. C., Stumpe, M. C., Van Cleve, J. E., et al. 2012, *PASP*, **124**, 1000

Soderblom, D. R. 2010, *ARA&A*, **48**, 581

Stauffer, J. R., Schultz, G., & Kirkpatrick, J. D. 1998, *ApJL*, **499**, L199

Stumpe, M. C., Smith, J. C., Catanzarite, J. H., et al. 2014, *PASP*, **126**, 100

Stumpe, M. C., Smith, J. C., Van Cleve, J. E., et al. 2012, *PASP*, **124**, 985

Thompson, S. E., Coughlin, J. L., Hoffman, K., et al. 2017, Planetary Candidates Observed by Kepler. VIII. A Fully Automated Catalog With Measured Completeness and Reliability Based on Data Release 25, [arXiv:1710.06758](https://arxiv.org/abs/1710.06758)

Torres, G., Andersen, J., & Giménez, A. 2010, *A&A Rev*, **18**, 67

Torres, G., Sandberg Lacy, C. H., Pavlovski, K., et al. 2014, *ApJ*, **797**, 31

von Boetticher, A., Triaud, A. H. M. J., Queloz, D., et al. 2017, *A&A*, **604**, L6

West, A. A., Hawley, S. L., Bochanski, J. J., et al. 2008, *ApJ*, **135**, 785

Wilson, J. C., Hearty, F., Skrutskie, M. F., et al. 2010,
in Proc. SPIE, Vol. 7735, Ground-based and
Airborne Instrumentation for Astronomy III,
77351C

Wilson, J. C., Hearty, F., Skrutskie, M. F., et al. 2012,
in Proc. SPIE, Vol. 8446, Ground-based and
Airborne Instrumentation for Astronomy IV,
84460H

Wright, E. L., Eisenhardt, P. R. M., Mainzer, A. K.,
et al. 2010, [AJ, 140, 1868](#)

Zasowski, G., Cohen, R. E., Chojnowski, S. D., et al.
2017, [AJ, 154, 198](#)

Zucker, S. 2003, [MNRAS, 342, 1291](#)